

# Structural Insights into Ligand Dynamics: Correlated Oxygen and Picket Motion in Oxycobalt Picket Fence Porphyrins

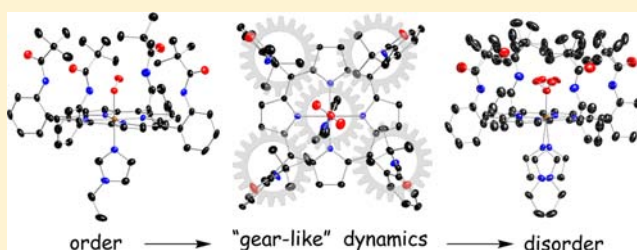
Jianfeng Li,<sup>†,‡</sup> Bruce C. Noll,<sup>‡</sup> Allen G. Oliver,<sup>‡</sup> and W. Robert Scheidt<sup>\*,‡</sup>

<sup>†</sup>College of Materials Science and Opto-electronic Technology, Graduate University of Chinese Academy of Sciences, 19A Yuquan Road, Beijing 100049, China

<sup>‡</sup>The Department of Chemistry and Biochemistry, University of Notre Dame, Notre Dame, Indiana 46556, United States

**S** Supporting Information

**ABSTRACT:** Two different oxygen-ligated cobalt porphyrins have been synthesized and the solid-state structures have been determined at several temperatures. The solid-state structures provide insight into the dynamics of Co–O<sub>2</sub> rotation and correlation with protecting group disorder. [Co(TpivPP)(1-EtIm)(O<sub>2</sub>)] (TpivPP = picket fence porphyrin) is prepared by oxygenation of [Co(TpivPP)(1-EtIm)<sub>2</sub>] in benzene solution. The structure at room temperature has the oxygen ligand within the ligand binding pocket and disordered over four sites and the trans imidazole is disordered over two sites. The structure at 100 K, after the crystal has been carefully annealed to yield a reversible phase change, is almost completely ordered. The phase change is reversed upon warming the crystal to 200 K, whereupon the oxygen ligand is again disordered but with quite unequal populations. Further warming to 300 K leads to greater disorder of the oxygen ligands with nearly equal O<sub>2</sub> occupancies at all four positions. The disorder of the *tert*-butyl groups of the protecting pickets is correlated with rotation of the O<sub>2</sub> around the Co–O(O<sub>2</sub>) bond. [Co(TpivPP)(2-MeHIm)(O<sub>2</sub>)] is synthesized by a solid-state oxygenation reaction from the five-coordinate precursor [Co(TpivPP)(2-MeHIm)]. Exposure to 1 atm of O<sub>2</sub> leads to incomplete oxygenation, however, exposure at 5 atm yields complete oxygenation. Complete oxygenation leads to picket disorder whereas partial (40%) oxygenation does not. Crystallinity is retained on complete degassing of oxygen in the solid, and complete ordering of the pickets is restored. The results should provide basic information needed to better model M–O<sub>2</sub> dynamics in protein environments.



## ■ INTRODUCTION

An understanding of the dynamics of the interactions of diatomics with hemes and heme proteins has long been considered fundamental to understanding function.<sup>1</sup> Mössbauer spectroscopy results have shown that the dynamics of the dioxygen complexes of hemes and heme proteins are especially rich. The temperature dependence of the quadruple splitting of oxyhemoglobin is an unusual and distinctive feature.<sup>2</sup> The picket fence derivative [Fe(TpivPP)(1-MeIm)(O<sub>2</sub>)]<sup>3</sup> also displayed anomalous line widths and quadrupole splittings in its Mössbauer spectra that were interpreted by Lang and co-workers as resulting from multiple configurations of the Fe–O<sub>2</sub> unit because of rotation around the Fe–O bond.<sup>4</sup> Later, Oldfield proposed a different model to explain the anomalous temperature-dependent line width behavior for the Mössbauer spectra; the model also required rotations around the Fe–O bond.<sup>5</sup> The Co–O<sub>2</sub> group in analogous cobalt complexes has similar dynamics that have been investigated by EPR.<sup>6a</sup> Rotation about the Co–O bond was observed both in small molecule as well as in hemoglobin derivatives.<sup>7</sup> Given these interesting ligand dynamics, we thought that a series of multiple-temperature X-ray studies could provide information on the ligand rotations, much like those we were able to map out for several six-coordinate nitrosyl iron porphyrins.<sup>8,9</sup> In

these cases, the lower temperature structures resolved disorder, even though the rotation about the axial Fe–N bond is a very low barrier process.

Accordingly, we carried out temperature-dependent structural investigations for both iron and cobalt dioxygen-ligated derivatives of picket fence porphyrin. These have included analogues for both R- and T-state hemoglobin and cobaltohemoglobin. Although the low-temperature structure determinations have substantially improved the available structural details of oxygen complexes, the studies have only partially resolved the disorder/dynamic structural issues. The results from the cobalt derivatives are the most illuminating and provide new information on the interaction between the axial oxygen ligand and the protecting pickets of the porphyrin. We present results from two series, [Co(TpivPP)(1-EtIm)(O<sub>2</sub>)] and [Co(TpivPP)(2-MeHIm)(O<sub>2</sub>)], both of which illustrate distinct features of the interactions between O<sub>2</sub> and the pickets. We will report results for three iron series members subsequently.<sup>10</sup>

Received: April 11, 2012

Published: May 30, 2012

## EXPERIMENTAL SECTION

**General Information.** All reactions and manipulations were carried out under argon using a double-manifold vacuum line, Schlenkware, and cannula techniques. Benzene, THF, and heptane were distilled over sodium/benzophenone and ethanol over magnesium. Research grade oxygen (99.999%) was purchased from PRAXAIR and used as received.  $[\text{H}_2(\text{TpivPP})]$  and  $[\text{Co}(\text{TpivPP})]$  were prepared according to a local modification of the reported syntheses;<sup>11</sup> additional information is in the Supporting Information. UV–vis spectra were recorded on a Perkin-Elmer Lambda 19 UV/vis/near-IR spectrometer.

**Synthesis of  $[\text{Co}(\text{TpivPP})(1\text{-EtIm})(\text{O}_2)]$ .** A chemical structure drawing is given in the Supporting Information.  $[\text{Co}(\text{TpivPP})(1\text{-EtIm})]$  was prepared by the reaction of  $\text{Co}(\text{TpivPP})$  (80 mg, 0.075 mmol) with excess 1-EtIm (0.06 mL, 0.60 mmol) in benzene.<sup>12</sup> A red crystalline powder was obtained by slow introduction of heptane into the benzene solution over 2–3 h.  $[\text{Co}(\text{TpivPP})(1\text{-EtIm})]$  (21.3 mg, 0.018 mmol) was dried under vacuum in a 50-mL Schlenk apparatus for 30 min. Drops of 1-ethylimidazole and benzene (~5 mL) were then transferred into the Schlenk apparatus by cannula. This mixture was gently heated with stirring and cooled to room temperature to give a clear red solution. Oxygen was then bubbled into this solution for 5 min. X-ray quality crystals were obtained in 8 mm  $\times$  250 mm sealed glass tubes by liquid diffusion using heptane as nonsolvent.

**Synthesis of  $[\text{Co}(\text{TpivPP})(2\text{-MeHIm})(\text{O}_2)]$ .**  $[\text{Co}(\text{TpivPP})(2\text{-MeHIm})]$  was prepared as described previously.<sup>12</sup> Moderate-size single crystals of  $[\text{Co}(\text{TpivPP})(2\text{-MeHIm})]$  were exposed at room temperature to pure dioxygen gas saturated with ethanol vapor. Crystals were obtained from exposure to (a) a ~1 atm dioxygen atmosphere for 3 days or (b) to a ~5 atm dioxygen atmosphere for 5 days in a high pressure reaction cylinder (Parr Instrument; Model 4635). After the oxygenation, the adducts were rapidly moved into the low temperature (100 K) nitrogen stream for structural characterization.

**X-ray Structure Determinations.** Single-crystal experiments were carried out on a Bruker Apex II system with graphite-monochromated Mo  $K\alpha$  radiation ( $\lambda = 0.71073 \text{ \AA}$ ) and a 700 Series Oxford Cryostream. The structures were solved by direct methods using SHELXS<sup>13</sup> and refined against  $F^2$  using SHELXL;<sup>13,14</sup> subsequent difference Fourier syntheses led to the location of most of the remaining non-hydrogen atoms. For the structure refinement, all data were used, including negative intensities. All non-hydrogen atoms were refined anisotropically if not remarked otherwise below. Hydrogen atoms were idealized with the standard SHELXL idealization methods. The programs SADABS<sup>15</sup> and TWINABS<sup>16</sup> were used to apply absorption corrections. Solid-state analysis of crystal packing distances made use of the program MERCURY<sup>17</sup> from the Cambridge Crystallographic Data Centre. Complete crystallographic details, atomic coordinates, anisotropic thermal parameters, and fixed hydrogen atom coordinates are given in the Supporting Information.

**$[\text{Co}(\text{TpivPP})(1\text{-EtIm})(\text{O}_2)]\cdot\text{C}_6\text{H}_6$ .** The complexes displayed differing structural features depending on the thermal history and are thus described in some detail. A freshly isolated crystal with dimensions  $0.39 \times 0.26 \times 0.19 \text{ mm}^3$  was picked for the temperature-dependent structure analysis. The crystal was glued to the tip of a thin glass fiber and quickly moved into the 100 K  $\text{N}_2$  stream (flash cooling). The crystal was found to be in the monoclinic crystal system with  $C2/c$  as the space group. The asymmetric unit contains half a picket fence porphyrin complex, and half a benzene solvent molecule. There is a crystallographic 2-fold axis passing through the coordinated oxygen (O1) and the cobalt (Co1) atoms and the axial 1-ethylimidazole ligand. The disordered, symmetry-related imidazoles were defined with a rigid group refinement with an ideal 1-ethylimidazole group.<sup>18</sup> For each “picket”, the pivalamido methyl carbon atoms were found to be disordered into two sets of positions. An ideal tetrahedral rigid group<sup>19</sup> was applied to constrain each *tert*-butyl group. The occupancies of the two independent pairs of *tert*-butyl groups are refined to 0.543(13) (C20, C21, C22, and C23) and 0.457(13) (C20B, C21B, C22B, and C23B); 0.555(5) (C24, C25, C26, and C27) and 0.445(5) (C24B,

C25B, C26B, and C27B). The terminal oxygen atom (O2) has a single crystallographically independent position and thus exhibits 2-fold positional disorder. The solvent benzene molecule has a 2-fold axis with an occupancy of a half molecule per asymmetric unit.

The crystal was then slowly warmed, in the  $\text{N}_2$  stream, to 188 K at a speed of 120 K/h and was allowed to stand for 30 min at 188 K. The crystal was then cooled back to 100 K at a rate of 120 K/h (ramp cooling). The crystal system was then observed to have changed to the lower symmetry of primitive triclinic. There are two twin domains with a rotation of  $179.9^\circ$  with rotation around the 110 reciprocal axis with a twin ratio of 64:36, and TWINABS<sup>16</sup> was used for the absorption correction. After data collection at 100 K, the structural analysis was carried out with the space group  $P\bar{1}$ . The asymmetric unit of structure now contains one complete picket fence porphyrin complex and one benzene solvent molecule. These molecules are ordered, including completely ordered picket *tert*-butyl groups. The only disorder observed was that of the terminal oxygen atom, which occupies two crystallographically independent positions with very different refined occupancies of 0.816(6) (O2A) and 0.184(6) (O2B).

The (same) crystal was then warmed to 200 K, X-ray data for the structure determination were collected, and then the crystal was warmed to 300 K and diffraction data were again collected. The same heating speed of 120 K/h was used. At both temperatures, the monoclinic crystal system and the  $C2/c$  space group were found. Similar crystal structure models and refinement procedures as those used originally ( $C2/c$ , 100 K) were applied. Disorder models for the *tert*-butyl pickets and axial imidazole ligand (2-fold symmetry) were applied as before. There is one significant difference, the terminal oxygen atom now occupies two crystallographically independent positions and thus exhibits approximate 4-fold positional disorder. The occupancy factors of the two unique oxygen positions were refined by means of “free variables”, and the final site occupancy factors were found to be 0.41(1) (O2A) and 0.09(1) (O2B) (200 K) and 0.27(1) (O2A) and 0.23(1) (O2B) (300 K).

This unusual thermal behavior was verified with a second crystal with dimensions  $0.34 \times 0.26 \times 0.18 \text{ mm}^3$ . When flash cooled to 100 K, the crystal again showed space group  $C2/c$ . After several annealing processes, the structure displayed the  $P\bar{1}$  space group. The detailed experimental process with crystallographic information and the thermal ellipsoid plot of  $[\text{Co}(\text{TpivPP})(1\text{-EtIm})(\text{O}_2)]\cdot\text{C}_6\text{H}_6$  ( $P\bar{1}$ , measured at 80 K) are given in the Supporting Information.

**$[\text{Co}(\text{TpivPP})(2\text{-MeHIm})(\text{O}_2)]$ .** The first experiment used a crystal (A) with dimensions  $0.50 \times 0.22 \times 0.21 \text{ mm}^3$  that had been reacted under a ~1 atm dioxygen atmosphere. After the oxygenation, the crystal was rapidly moved to a diffractometer under a 100 K nitrogen stream, and X-ray data were collected. This crystal sample was found to be incompletely oxygenated.

A second crystal (B) with the dimensions  $0.37 \times 0.21 \times 0.16 \text{ mm}^3$  was oxygenated under a ~5 atm dioxygen atmosphere. After oxygenation, which was complete, the crystal was rapidly moved to the diffractometer under a 100 K nitrogen stream and structural data collected. After the 100 K data collection, the crystal was slowly warmed to 300 K at 120 K/h under the  $\text{N}_2$  stream. Then the structural data were collected at 300 K.

The crystallographic data for all data sets was consistent with that of the monoclinic crystal system and space group  $C2/c$ ; this is the same crystal system and space group as that of the five-coordinate precursor  $[\text{Co}(\text{TpivPP})(2\text{-MeHIm})]$ . There is a crystallographic 2-fold axis passing through the coordinated oxygen (O1) and the cobalt (Co1) atoms. The 2-methylimidazole ligand is disordered between two symmetry related sites. The terminal oxygen atom (O2) occupies one crystallographically independent position, and thus, it exhibits 2-fold positional disorder. The occupancy of the dioxygen ligand was carefully judged from the crystallographic results. First, the applied occupancy factor should give reasonable anisotropic displacement parameters (ADPs) compared to those of other atoms in the same molecule. Second, the command of “FMAP-2” was applied to examine the resulting Fourier difference maps, especially the holes and peaks around the positions of dioxygen atoms. After careful refinement, the occupancies of dioxygen were set at 0.4 (crystal A), 1.0 (crystal B, 100

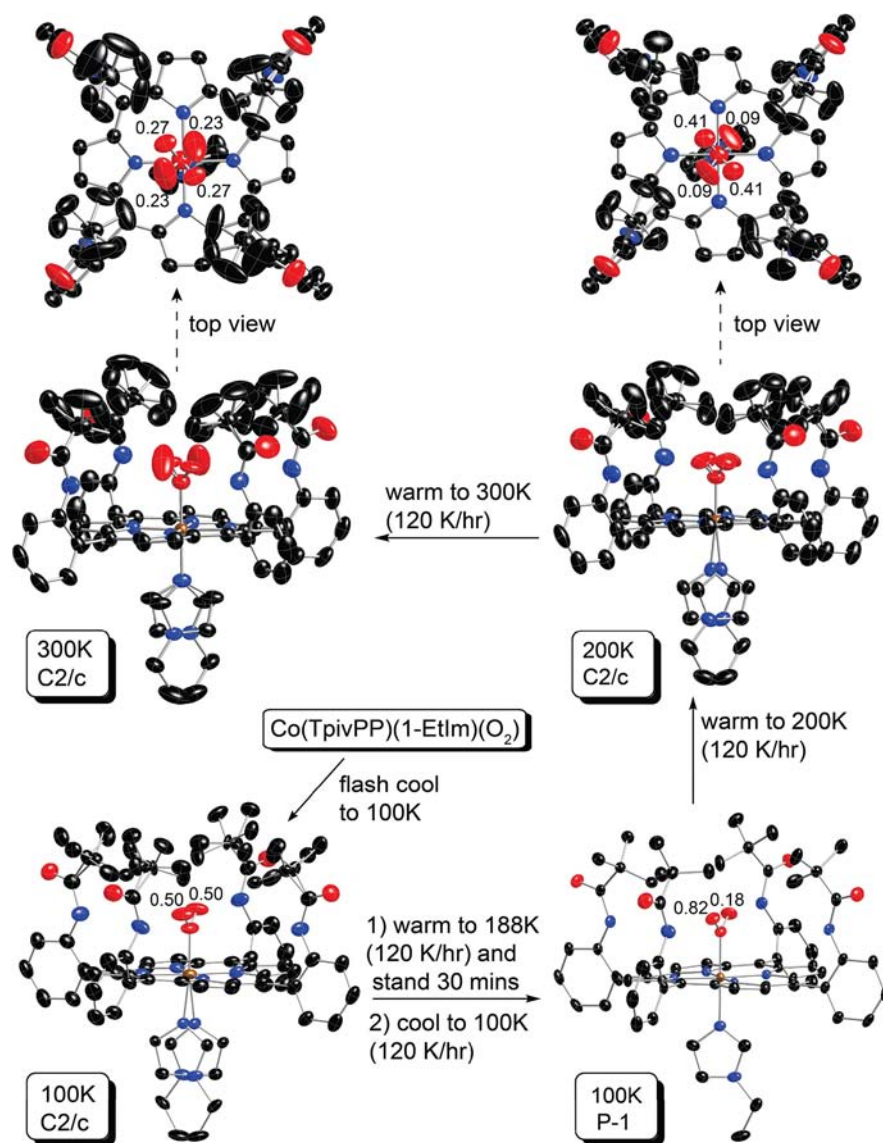


**Figure 1.** Thermal ellipsoid diagrams of the  $[\text{Co}(\text{TpivPP})(1\text{-EtIm})(\text{O}_2)]$  structure at 100, 200, and 300 K, showing the thermally dependent history. The temperature and corresponding space group are given in the highlighted boxes. Both orientations are shown for the axial imidazole when disordered over two positions. The terminal oxygen populations are also indicated. Thermal ellipsoids are contoured at the 50% probability level for the 100 K result, 40% for the 200 K result, and 30% for the 300 K result. Hydrogens are omitted for clarity. Two views are given for the 200 and 300 K structures to allow better views of the  $\text{O}_2$  disorder.

K), and 0.3 (crystal B, 300 K). Two ethanol solvent molecules are found, and each is disordered around a 2-fold axis. In each structure, the first ethanol molecule is fully occupied; the second ethanol molecule occupancy was found to be 1, 0.8, and 0.8, respectively. Hence, the three structures are  $[\text{Co}(\text{TpivPP})(2\text{-MeHIm})0.4(\text{O}_2)] \cdot 2\text{C}_2\text{H}_5\text{OH}$  (100 K, crystal A),  $[\text{Co}(\text{TpivPP})(2\text{-MeHIm})(\text{O}_2)] \cdot 1.8\text{C}_2\text{H}_5\text{OH}$  (100 K, crystal B),  $[\text{Co}(\text{TpivPP})(2\text{-MeHIm})0.3(\text{O}_2)] \cdot 1.8\text{C}_2\text{H}_5\text{OH}$  (300 K, crystal B), respectively.

After the 300 K data collection, crystal B (characterized as  $[\text{Co}(\text{TpivPP})(2\text{-MeHIm})0.3(\text{O}_2)]$ ) was moved into an argon atmosphere that was saturated with ethanol vapor. Every 12 h, the sample cylinder was pumped slightly and refilled for several cycles to keep a pure argon atmosphere. Two days later, the crystal was used for a final structural characterization. The crystal was rapidly moved to a 100 K nitrogen stream and structural data collected. In this structure, the asymmetric unit contains half a picket fence porphyrin complex and two half-ethanol solvent molecules. There is a crystallographic 2-fold axis passing through the cobalt atom. The 2-methylimidazole ligand was found to disorder between two 2-fold related sites. Each

solvent ethanol molecule also possesses a 2-fold axis. The crystalline molecule has thus reverted to  $[\text{Co}(\text{TpivPP})(2\text{-MeHIm})] \cdot 1.8\text{C}_2\text{H}_5\text{OH}$ .

## RESULTS

The synthesis and molecular structure characterizations of two oxycobalt(II) picket fence porphyrin complexes are reported. The molecular structure determinations have been carried out at a variety of temperatures between 100 and 300 K. The first is six-coordinate  $[\text{Co}(\text{TpivPP})(1\text{-EtIm})(\text{O}_2)]$ , which was synthesized and crystallized from solution. The second,  $[\text{Co}(\text{TpivPP})(2\text{-MeHIm})(\text{O}_2)]$ , utilizing sterically hindered 2-methylimidazole, was synthesized from the heterogeneous reaction of gaseous dioxygen and crystalline, five-coordinate  $[\text{Co}(\text{TpivPP})(2\text{-MeHIm})]$ . Difficulties with incomplete oxygenation are noted.

**$[\text{Co}(\text{TpivPP})(1\text{-EtIm})(\text{O}_2)]$ .** The synthesis of  $[\text{Co}(\text{TpivPP})(1\text{-EtIm})(\text{O}_2)]$  is similar to that of  $[\text{Fe}(\text{TpivPP})(1\text{-MeIm})(\text{O}_2)]$ , but the precursor is five-coordinate  $[\text{Co}(\text{TpivPP})(1\text{-$

**Table 1. Complete Crystallographic Details for [Co(TpivPP)(1-EtIm)(O<sub>2</sub>)]·C<sub>6</sub>H<sub>6</sub> at 100, 200, and 300 K (All Measurements Were Conducted on the Same Crystal)**

	sample treatment			
	flash cooled	after annealing	warm to 200 K	warm to 300 K
chemical formula	C <sub>75</sub> H <sub>78</sub> CoN <sub>10</sub> O <sub>6</sub>	C <sub>75</sub> H <sub>78</sub> CoN <sub>10</sub> O <sub>6</sub>	C <sub>75</sub> H <sub>78</sub> CoN <sub>10</sub> O <sub>6</sub>	C <sub>75</sub> H <sub>78</sub> CoN <sub>10</sub> O <sub>6</sub>
FW	1274.40	1274.40	1274.40	1274.40
<i>a</i> , Å	18.586(4)	13.0971(9)	18.5681(7)	18.711(2)
<i>b</i> , Å	19.170(4)	13.5557(9)	19.2564(8)	19.566(3)
<i>c</i> , Å	18.316(4)	18.2431(12)	18.4497(7)	18.725(3)
$\alpha$ , deg	90	89.216(4)	90	90
$\beta$ , deg	90.25(3)	88.444(3)	90.169(2)	90.824(5)
$\gamma$ , deg	90	88.190(3)	90	90
<i>V</i> , Å <sup>3</sup>	6526(2)	3235.8(4)	6596.7(4)	6854.6(17)
<i>V</i> , Å <sup>3</sup> /molecule	1632	1617.9	1649.2	1713.8
space group	C2/ <i>c</i>	P $\bar{1}$	C2/ <i>c</i>	C2/ <i>c</i>
<i>Z</i>	4	2	4	4
temp, K	100	100	200	300
<i>D</i> <sub>calcd</sub> , g cm <sup>-3</sup>	1.297	1.308	1.283	1.235
$\mu$ , mm <sup>-1</sup>	0.326	0.328	0.322	0.310
final <i>R</i> indices	<i>R</i> <sub>1</sub> = 0.0477	<i>R</i> <sub>1</sub> = 0.0496	<i>R</i> <sub>1</sub> = 0.0486	<i>R</i> <sub>1</sub> = 0.0606
[ <i>I</i> > 2 $\sigma$ ( <i>I</i> )]	<i>wR</i> <sub>2</sub> = 0.1139	<i>wR</i> <sub>2</sub> = 0.1276	<i>wR</i> <sub>2</sub> = 0.1266	<i>wR</i> <sub>2</sub> = 0.1755
final <i>R</i> indices	<i>R</i> <sub>1</sub> = 0.0783	<i>R</i> <sub>1</sub> = 0.0744	<i>R</i> <sub>1</sub> = 0.0911	<i>R</i> <sub>1</sub> = 0.1091
(all data)	<i>wR</i> <sub>2</sub> = 0.1226	<i>wR</i> <sub>2</sub> = 0.1466	<i>wR</i> <sub>2</sub> = 0.1498	<i>wR</i> <sub>2</sub> = 0.2052

**Table 2. Complete Crystallographic Details for [Co(TpivPP)(2-MeHIm)] and Its Oxygenated Derivatives**

	[Co(TpivPP)(2-MeHIm) 0.4(O <sub>2</sub> )]·2C <sub>2</sub> H <sub>5</sub> OH	[Co(TpivPP)(2-MeHIm) (O <sub>2</sub> )]·1.8C <sub>2</sub> H <sub>5</sub> OH	[Co(TpivPP)(2-MeHIm) 0.3(O <sub>2</sub> )]·1.8C <sub>2</sub> H <sub>5</sub> OH	[Co(TpivPP)(2-MeHIm) ·1.8C <sub>2</sub> H <sub>5</sub> OH
chemical formula	C <sub>72</sub> H <sub>82</sub> CoN <sub>10</sub> O <sub>6.8</sub>	C <sub>71.6</sub> H <sub>80.8</sub> CoN <sub>10</sub> O <sub>7.8</sub>	C <sub>71.6</sub> H <sub>80.8</sub> CoN <sub>10</sub> O <sub>6.4</sub>	C <sub>71.6</sub> H <sub>82</sub> CoN <sub>10</sub> O <sub>5.8</sub>
FW	1255.21	1265.19	1242.79	1234.40
<i>a</i> , Å	18.5678(7)	18.7514(3)	18.9063(5)	18.6326(3)
<i>b</i> , Å	19.5594(8)	19.5309(3)	19.6633(5)	19.6158(3)
<i>c</i> , Å	17.8219(6)	17.8719(3)	18.3473(5)	17.9050(3)
$\alpha$ , deg	90	90	90	90
$\beta$ , deg	90.954(2)	91.065(1)	91.666(1)	90.879(1)
$\gamma$ , deg	90	90	90	90
<i>V</i> , Å <sup>3</sup>	6471.6(4)	6544.13(18)	6817.9(3)	6543.39(18)
space group	C2/ <i>c</i>	C2/ <i>c</i>	C2/ <i>c</i>	C2/ <i>c</i>
<i>Z</i>	4	4	4	4
temp, K	100	100	300	100
<i>D</i> <sub>calcd</sub> , g cm <sup>-3</sup>	1.288	1.284	1.211	1.253
$\mu$ , mm <sup>-1</sup>	0.328	0.326	0.310	0.322
final <i>R</i> indices	<i>R</i> <sub>1</sub> = 0.0509	<i>R</i> <sub>1</sub> = 0.0559	<i>R</i> <sub>1</sub> = 0.0758	<i>R</i> <sub>1</sub> = 0.0572
[ <i>I</i> > 2 $\sigma$ ( <i>I</i> )]	<i>wR</i> <sub>2</sub> = 0.1399	<i>wR</i> <sub>2</sub> = 0.1591	<i>wR</i> <sub>2</sub> = 0.2301	<i>wR</i> <sub>2</sub> = 0.1633
final <i>R</i> indices	<i>R</i> <sub>1</sub> = 0.0593	<i>R</i> <sub>1</sub> = 0.0676	<i>R</i> <sub>1</sub> = 0.1219	<i>R</i> <sub>1</sub> = 0.0733
(all data)	<i>wR</i> <sub>2</sub> = 0.1512	<i>wR</i> <sub>2</sub> = 0.1703	<i>wR</i> <sub>2</sub> = 0.2646	<i>wR</i> <sub>2</sub> = 0.1776

EtIm)]<sup>12</sup> instead of six-coordinate [Fe(TpivPP)(1-MeIm)<sub>2</sub>]. Crystals of [Co(TpivPP)(1-EtIm)(O<sub>2</sub>)] containing the six-coordinate porphyrinate and benzene solvate have been characterized at various temperatures and cooling regimes. Thermal ellipsoid diagrams of the molecular structure at different temperatures and thermal history are given in Figure 1. A brief summary of the crystallographic data is given in Table 1, and complete crystallographic details, atomic coordinates, bond distances, and bond angles of the structure are given in Tables S1–S24 of the Supporting Information.

In the process of the structural characterization of [Co(TpivPP)(1-EtIm)(O<sub>2</sub>)], we observed that the low-temperature structure (100 K) is different depending on the cooling process for the specimen. When a fresh crystal is quickly cooled to 100 K in the N<sub>2</sub> stream (flash cooling), the crystals are found

in the monoclinic crystal system, whereas when a crystal is annealed and then slowly cooled to 100 K, the crystal displays triclinic diffraction symmetry (Figure 1). This behavior appears to be both reversible and reproducible. The monoclinic crystal form is found in the centrosymmetric space group C2/*c* with required 2-fold symmetry for the molecule, and as will be discussed subsequently, the molecule has disordered axial ligands and disordered pickets. In contrast, the triclinic crystal form has no required crystallographic symmetry, completely ordered pickets and axial imidazole, and only minor disorder of the axial O<sub>2</sub> ligand. The terminal oxygen atom occupies two crystallographically independent positions with occupancies refined to be 0.816(6) (O2A) and 0.184 (O2B).

When the same crystal was warmed to 200 K and then to 300 K (120 K/h), the crystal was again found in the monoclinic

**Table 3. Coordination Group and Picket Parameters for [Co(TpivPP)(1-EtIm)(O<sub>2</sub>)] and [Co(TpivPP)(2-MeHIm)(O<sub>2</sub>)] at Differing Temperatures and Conditions**

compd	cryst form	T, K	Co–O <sup>a</sup>	Co–N <sub>p</sub> <sup>a,b</sup>	Co–N <sub>im</sub> <sup>a</sup>	O–O <sup>a</sup>	Co–O–O <sup>c</sup>	O–Co–N <sub>im</sub> <sup>c</sup>	picket config <sup>d</sup>	no. imid orient. <sup>e</sup>	no. O <sub>2</sub> orient. <sup>f</sup>
A. Related to [Co(TpivPP)(1-EtIm)(O <sub>2</sub> )]											
[Co(TPP)(1-MeIm)] <sup>g</sup>		295		1.977(6)	2.157(3)					1	
[Co(TpivPP)(1-EtIm)(O <sub>2</sub> )]	P $\bar{1}$	100	1.9029(19)	1.978(3)	2.017(2)	1.239(3)	120.3(2)	178.20(11)	4Ord	1	2
[Co(TpivPP)(1-EtIm)(O <sub>2</sub> )]	C2/c	100	1.899(2)	1.9895(6)	2.032(2)	1.116(4)	127.5(2)	173.44(11) <sup>h</sup>	4Dis	2	2
[Co(TpivPP)(1-EtIm)(O <sub>2</sub> )]	C2/c	200	1.899(2)	1.9739(2)	2.0293(18)	1.131(5)	127.4(3)	173.71(8) <sup>h</sup>	4Dis	2	4
[Co(TpivPP)(1-EtIm)(O <sub>2</sub> )]	C2/c	300	1.942(4)	1.980(2)	2.046(2)	1.13(2)	128.7(14)	180 <sup>h,i</sup>	4Dis	2	4
[Co(TpivPP)(1-EtIm)(O <sub>2</sub> )]#2	P $\bar{1}$	80	1.929(6)	1.982(9)	2.029(6)	1.129(9)	128.0(6)	179.2(4)	4Ord	1	2
B. Related to [Co(TpivPP)(2-MeHIm)(O <sub>2</sub> )]											
[Co(TpivPP)(2-MeHIm)] <sup>j</sup>	C2/c	100		1.979(3)	2.145(3)				4Ord	2	
[Co(TpivPP)(2-MeHIm)0.4(O <sub>2</sub> )]	C2/c	100	1.934(6)	1.9751(12)	2.108(3)	1.100(9)	128.8(6)	173.81(15) <sup>h</sup>	4Ord	2	2
[Co(TpivPP)(2-MeHIm)(O <sub>2</sub> )]	C2/c	100	1.902(2)	1.9850(16)	2.078(2)	1.110(4)	128.8(2)	173.93(8) <sup>h</sup>	4Dis	2	2
[Co(TpivPP)(2-MeHIm)0.3(O <sub>2</sub> )]	C2/c	300	1.993(9)	1.986(3)	2.153(5)	0.98(2)	139.3(16)	173.10(16) <sup>h</sup>	4Ord?	2	2
[Co(TpivPP)(2-MeHIm)]	C2/c	100		1.983(4)	2.158(3)				4Ord	2	
[Co(TPP)(1,2-Me <sub>2</sub> Im)] <sup>k</sup>		295		1.985(3)	2.216(2)					1	

<sup>a</sup>Values in angstroms. <sup>b</sup>Averaged value. <sup>c</sup>Values in degrees. <sup>d</sup>Number of pickets ordered (Ord) and/or disordered (Dis). <sup>e</sup>Number of imidazole orientations. <sup>f</sup>Number of O<sub>2</sub> orientations. <sup>g</sup>Values from ref 54. <sup>h</sup>The differences between 180° and the observed angle represent the off-axis tilt of the imidazole. <sup>i</sup>Not resolved. <sup>j</sup>Values from ref 12. <sup>k</sup>Values from ref 55.

crystal system in space group C2/c. The axial imidazole, the dioxygen ligand, and the pickets display increasingly serious disorder as the temperature is increased, as displayed in Figure 1; the occupancy ratios of the 4-fold disordered dioxygen ligands are 0.41:0.09 (200 K) and 0.27:0.23 (300 K).

**[Co(TpivPP)(2-MeHIm)(O<sub>2</sub>)].** When crystalline [Co(TpivPP)(2-MeHIm)] is exposed to oxygen at 1 atm, the five-coordinate complex becomes partially oxygenated. The crystal structure analysis suggests that the oxygenation reaction is about 40% complete. Oxygenation at 5 atm leads to complete oxygenation, [Co(TpivPP)(2-MeHIm)(O<sub>2</sub>)], that retains all oxygen at 100 K, but molecular oxygen is slowly lost from the single crystal at temperatures above ~200 K. The structure determined at 300 K showed about 30% occupancy of the remaining coordinated O<sub>2</sub>. The complex can be completely deoxygenated, and the structure of such a crystal shows no apparent degradation. A brief summary of the crystallographic data of the 2-MeHIm structures is given in Table 2, and complete crystallographic details, atomic coordinates, bond distances, and bond angles of these four structures are given in Tables S25–S48 of the Supporting Information.

## DISCUSSION

The picket fence dioxygen complexes have crystallographically imposed 2-fold symmetry leading to disorder of the bent dioxygen ligand and the trans imidazole ligand. In addition, a

second crystallographically independent position of the dioxygen is found. Thus, the coordinated dioxygen displays 4-fold disorder and the trans imidazole 2-fold disorder. Interestingly, the disorder of the pickets, found in the dioxygen picket fence complexes, is not a common phenomenon with pocket ligands other than dioxygen, suggesting that the pickets are not “inert” with respect to the dioxygen ligand.

Even though an individual single-crystal X-ray analysis cannot discriminate between crystalline disorder caused by static phenomena or by dynamic processes occurring in the solid state, the use of multiple-temperature structure determinations on the same single-crystal specimen can yield substantial insight into the nature of possible dynamic processes. A series of iron(II) nitrosyl complexes showed how multiple-temperature X-ray structures could provide significant information into the pathways of NO ligand motion.<sup>8,9</sup> The striking success of the NO studies led us to carry out multiple-temperature studies of picket fence dioxygen complexes at a variety of temperatures from ambient down to 80–100 K. We have examined the structures of the cobalt(II) species on the expectation that useful information concerning the solid-state dynamics of the O<sub>2</sub> complexes would be obtained.

**Structure of [Co(TpivPP)(1-EtIm)(O<sub>2</sub>)].** The structure of [Co(TpivPP)(1-EtIm)(O<sub>2</sub>)] has been independently determined four times with differing temperatures and thermal

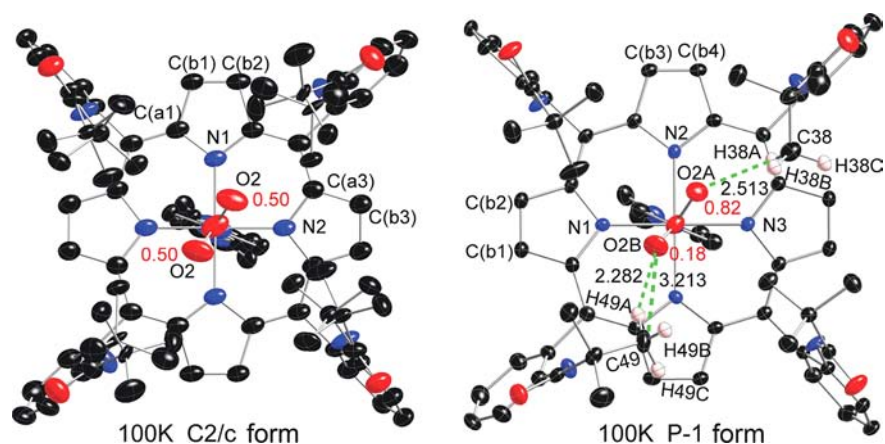


**Figure 2.** Top view thermal ellipsoid plots of two 100 K  $[\text{Co}(\text{TpivPP})(1\text{-EtIm})(\text{O}_2)]$  structures (left,  $C2/c$  form; right,  $P\bar{1}$  form) displaying the atom labeling scheme. The terminal oxygen populations are also indicated. In the 100 K  $P\bar{1}$  structure (right), the short contacts (dashed lines) and values between terminal oxygen (O2A and O2B) and picket atoms are shown. Thermal ellipsoids of all atoms in both structures are contoured at the 50% probability level. Hydrogen atoms have been omitted for clarity.

treatments, but all on the same crystal specimen. As shown in Table 3, the coordination group geometry parameters do not vary largely. Most of the differences are likely the consequence of the disorder issues described below, which do vary widely; values are given in Table 3. As will be discussed subsequently, some aspects of the thermal behavior were further studied on a second crystalline specimen that confirmed the general behavior.

When a freshly prepared crystal of  $[\text{Co}(\text{TpivPP})(1\text{-EtIm})(\text{O}_2)]$  is subjected to X-ray structure analysis using what are now routine, modern-day techniques, i.e., flash cooling the crystal to low temperature (typically 100 K) and then commencing the diffraction study, the crystals are observed in the space group  $C2/c$ . This space group leads to crystallographically imposed 2-fold symmetry and to 2-fold disorder in both axial ligands. However, unlike prior iron results,<sup>20,21</sup> the terminal oxygen is found only in the pair of positions related by the molecular 2-fold axis and not in another set of positions that led to effectively 4-fold disorder. Apparently, the relatively small differences between the  $\text{M}-\text{O}_2$  bonding of the cobalt dioxygen species and the analogous iron species lead to a significant difference in the disorder (dynamics) of the complexes.

A top down view of the cobalt complex is given in the left panel of Figure 2; additional thermal ellipsoid plots are given in Figures S2 and S3 of the Supporting Information. As can be seen in the left panel, even though the  $\text{O}_2$  only exhibits 2-fold disorder, all pickets are disordered, with each having two distinct orientations of the *tert*-butyl group; none of the picket disorder is a consequence of the crystallographic symmetry. Moreover, although there is no necessary crystallographic correlation between the orientational disorder of the pickets and the coordinated  $\text{O}_2$ , calculations suggested that picket behavior is intrinsically related to the oxygen ligand dynamics.<sup>22</sup> A close examination of Figure 2, or better Figure S2, shows details of the orientations of the *tert*-butyl groups. The disordered *tert*-butyl groups pointing toward the oxygen have two methyl groups oriented inward to the pocket cavity whereas the picket at the other site has only one methyl group inward to the pocket cavity. Each of the independent *tert*-butyl groups has two distinct but similar orientations, but the two pickets show distinct patterns. We will represent the orientation of the *tert*-butyl groups with the symbol “<o” for those with the

two methyl groups inward and bracketing the oxygen and those with the single inward methyl group as “>.”

The two sets of orientations of the two inward methyl groups (<o) interact almost equally with the terminal oxygen atom, effectively on each side of the oxygen. The contacts are  $\text{O2}\cdots\text{C27} = 3.26 \text{ \AA}$  and  $\text{O2}\cdots\text{C25} = 4.41 \text{ \AA}$  for the first picket orientation and  $\text{O2}\cdots\text{C25b} = 3.33 \text{ \AA}$  and  $\text{O2}\cdots\text{C27b} = 4.02 \text{ \AA}$  for the second picket orientation. There is an equivalent set of such interactions  $180^\circ$  away, as required by the 2-fold symmetry. The short  $\text{O}\cdots\text{C}$  distances are very near the van der Waals radii sum of  $3.22 \text{ \AA}$ .<sup>23</sup> The second set of disordered pickets have a single inward methyl group (>), and their positions are not directly affected by the presence of the oxygen ligand. Note that additional details of the picket interactions are given in the Supporting Information figures as appropriate.

The <o orientation has been commonly observed when the pocket ligand is not linear, for example, N-coordinated nitrite. In a number of iron(II) and -(III) nitrite picket fence derivatives,<sup>24</sup> the terminal nitrite oxygen atoms are bracketed by two methyl groups, but the pickets are completely ordered with a single orientation. One possible explanation for the two orientations of the picket bracketing the terminal oxygen of the coordinated  $\text{O}_2$  is that any rotation of  $\text{O}_2$  around the  $\text{Co}-\text{O}$  bond must be correlated with picket motion. That such an  $\text{O}_2$  rotation must be occurring in the solid state is shown by the experiments described below.

The disorder of the pickets, the  $\text{O}_2$ , and even the trans imidazole ligand is shown to be variable by the structures obtained at different temperatures and cooling conditions. As described in Figure 1 and the Experimental Section, when the crystal was annealed after cooling to 100 K, warming to 188 K, and then slowly recooling to 100 K, substantial structural change occurred. The crystallographic space group changed to  $P\bar{1}$ , leading to no required symmetry on the molecule, and the molecule itself is almost completely ordered. The four pickets all have a single orientation; the imidazole has a single orientation and not the two previously required. The coordinated oxygen molecule still has two orientations, but the terminal atom occupancies are decidedly asymmetric with occupancies of the major (O2a) atom at 0.816 (7) and the minor (O2b) at 0.184. The two  $\text{Co}-\text{O}-\text{O}$  planes are not quite coplanar. These features are all clearly seen in Figure 2 (right panel) and Figures S4 and S5 of the Supporting Information.

The picket orientation follows the same pattern as noted before (< *o* toward oxygen and > for the other pair), with comparable short C...O contacts (for O2a = 3.34 Å and O2b = 3.21 Å). In both 100 K structures, the Co–O–O planes have a near-perpendicular conformation with respect to the imidazole plane, suggesting that this orientation is the most favored one. Clearly, both the O<sub>2</sub> and imidazole groups have rotated around their coordinating bond during the annealing process. The rotation around the Co–O bond (in either direction) requires that the picket methyl groups must also move to lower the barrier. Thus, the dynamics and energetics of O<sub>2</sub> rotation depend on two distinct molecular features: the barrier to rotation around the Co–O bond and the energy required for the necessary movement of the pickets. It is likely that the picket disorder, which is seen as alternate orientations of the *tert*-butyl groups, is the likely “residue” from the Co–O<sub>2</sub> rotation. Correlated motion of the pickets and O<sub>2</sub> in a geared fashion are required to avoid impossible atom...atom contacts; the differing positions of the *tert*-butyl groups must be nearly energetically equivalent. However, the energetics of the picket orientation will depend on whether or not there is an O<sub>2</sub> ligand in proximity.

Additional interesting structural features are observed when the crystal is warmed to 200 K, which was accomplished without removal from the diffractometer. The space group reverts back to C2/c, with required 2-fold symmetry for the molecule, and the complex is again disordered. Indeed, additional disorder is observed with four terminal oxygen positions with the unique occupancy factors of 0.412 (11) and 0.088. The major occupancy Co–O–O planes remain nearly perpendicular to the imidazole plane. The features are illustrated in Figures 1, S6, and S7. The pickets associated with the major occupancy terminal oxygen again display a pair of < *o* conformations with the closest O...C contacts of 3.31 and 3.26 Å. Picket conformations associated with the minor occupancy oxygen atom are more complex, with both a < *o* and a > conformation. The nonbonded contact with the terminal oxygen and the closest carbon of the < *o* conformation is 3.14 Å, whereas the apparent O...C contact with the > picket conformation is an impossible 2.50 Å. It is to be noted that the apparent thermal motion of the minor occupancy oxygen atom is much more diffuse than that of the major occupancy oxygen atom. It is not clear whether this is a real phenomenon or an artifact of the least-squares refinement. We prefer the first explanation.

Further warming to 300 K continues the trend to increasing disorder. Figures 1, S8, and S9 display two views of the molecule. The terminal oxygen atoms again occupy four sites, but they now have nearly equal populations of 0.27 (2):0.23:0.27:0.23. The orientation of the pickets is also more diffuse. The orientations of the pickets for the (marginally) major orientation O2a are now less clear: one is clearly < *o*, but the other orientation verges on >; the close O...C contacts are 3.58 and 3.79 Å for the first picket orientation and 2.70 Å for the second. The picket orientations associated with the second oxygen atom (O2b) are both close to the > conformation with calculated shortest contacts of 2.59 and 2.98 Å. Although the thermal parameters (or more precisely the anisotropic displacement parameters) for all atoms have increased over the temperature range, those of the picket methyl groups have especially increased. As can be seen in Figure S8, the appearance of these thermal parameters suggests a near continuum of varying methyl group positions about the

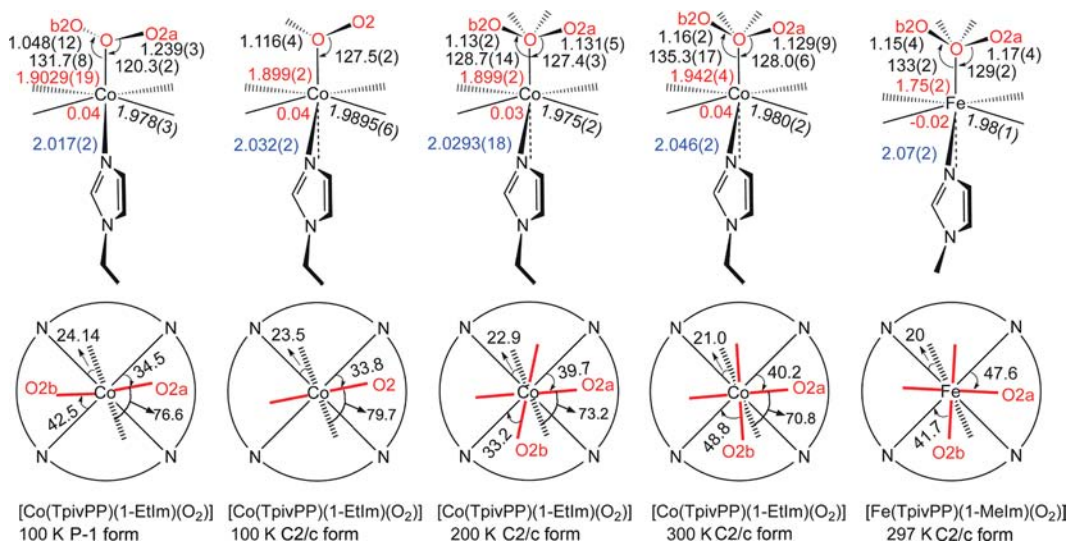
C<sub>*tert*-butyl</sub>–C<sub>amide</sub> bond and effectively appears close to free rotation at 300 K. The apparent easy movement of the pickets may be the reason that the oxygen atom occupancies are now near a statistical 0.25.

We have studied the reproducibility and other variations of the crystal annealing process on a second, independently prepared crystal of [Co(TpivPP)(1-EtIm)(O<sub>2</sub>)]. The sequence of conditions used to explore this temperature variability is given in Figure S10. The basic observations that were described above were found again. Flash cooling gave a crystal in space group C2/c with, as before, two orientations of the terminal oxygen atom. Annealing again gave a phase change and space group P1̄, with two asymmetrically occupied oxygen positions; however, disorder in all the pickets and a disordered imidazole were observed. Further annealing cycles, as shown in Figure S10, were followed by a final structure determination at 80 K. This result was nearly identical to the 100 K structure noted earlier, with ordered pickets and imidazole and asymmetric oxygen atom occupancies of 0.77(2) and 0.23; the O<sub>2</sub> occupancies are within two standard deviations of the first determination. An illustration of this independently determined structure is given in Figure S11.

We conclude that, in the absence of external constraints, the bent Co–O–O group would be equally populated in all four of the quadrants of the porphyrin core with jumps between each quadrant.<sup>25</sup> The temperature-dependent crystallographic studies of the picket fence derivatives clearly demonstrate that the location of the dioxygen ligand is the result of the constraints of the intramolecular interactions between the dioxygen and pickets. These constraints must control the oxygen motion and populations, with the constraints relaxing as the temperature increases. Although the lowest temperature structure after annealing is almost completely ordered, it is possible that more elaborate temperature cycling than we have been able to employ would lead to a single ordered Co–O<sub>2</sub> orientation.

Despite the variation of differing interactions in the ligand binding pocket in the four structures determined, the complex displays the same core conformation that indeed is almost quantitatively identical for all four structures. This is true even for the pair at 100 K that has undergone the phase change. Formal diagrams illustrating the atomic displacements, in units of 0.01 Å, from the mean 24-atom plane of the porphyrin are given in Figure S12. One interesting feature is that the cobalt atom is always slightly displaced from the mean plane toward the imidazole ligand and not the dioxygen ligand. Also shown are the averaged values of bond distances and angles in each of the four observed structures along with the value of the estimated standard deviation, calculated on the assumption that all averaged values are drawn from the same population.

Values of coordination group parameters, those for coordinated O<sub>2</sub>, and picket configuration are summarized in Table 3. Figure S12 gives values for core distances and angles and also displays the relative orientation of the axial ligands. The coordination group values compare well with those from earlier structure determinations of dioxygen cobalt complexes. The first X-ray characterized monomeric oxygen-carrying cobalt complex is the six-coordinate [Co(beacen)(Py)(O<sub>2</sub>)], reported at 1972 as a model for oxygenated hemoglobin.<sup>26</sup> The Co–O<sub>2</sub> distance and Co–O<sub>2</sub> angle were determined as 1.86 Å and 126°. Since then a number of cobalt–O<sub>2</sub> (1:1) structures have been published, most of which are also ligated to a Schiff base.<sup>27–32</sup> In these cobalt dioxygen structures, the O<sub>2</sub> group is frequently disordered.<sup>29</sup> In the relatively accurate low-temper-

Scheme 1. Formal Diagrams of Structures of  $[\text{Co}(\text{TpivPP})(1\text{-EtIm})(\text{O}_2)]$  at Different Temperatures and Space Groups<sup>a</sup>

<sup>a</sup>The upper panels are edge-on views of the porphyrin plane and ligands with key parameters (distances in Å, angle in deg) shown in the sequence O–O, O–O–M, M–O,  $\Delta_{24}$  (positive to imidazole ligand side), M–N<sub>p</sub>, and M–N<sub>ax</sub>. The lower panels are top views of the porphyrin plane showing the projections of the dioxygen (red line) and imidazole planes (dashed line) and their angles between the related M–N<sub>p</sub> vectors. Room temperature values for  $[\text{Fe}(\text{TpivPP})(1\text{-MeIm})(\text{O}_2)]$ <sup>20</sup> are also shown.

ature structures by Schaefer et al., the Co–O<sub>2</sub> distance and Co–O<sub>2</sub> angle are in the ranges 1.870(6)–1.889(2) Å and 116.4(5)–120.0(2)°. The dioxygen group is positioned between the Co–O and Co–N bonds<sup>30</sup> or bisects the N–Co–N angle of the Schiff base ligand.<sup>26</sup> Either arrangement allows for good overlap between  $\pi^*$  orbitals on the dioxygen group and  $d_x$  orbitals on the cobalt atom. There is a single oxycobalt porphyrin structure, also based on a picket fence, but with a trans thiolate ligand it has limited precision with a 2-fold disordered oxygen ligand.<sup>33</sup> Agreement between the differing oxycobalt structures is satisfactory.

The nearly complete ordering of the dioxygen ligand allows, for the first time to our knowledge, the possibility of looking for subtle asymmetry, caused by the O<sub>2</sub> ligand, in the structure of  $[\text{Co}(\text{TpivPP})(1\text{-EtIm})(\text{O}_2)]$ . Such asymmetry (an off-axis tilt of the diatomic ligand and unequal equatorial bond distances) had been observed in both five-coordinate<sup>34,35</sup> and six-coordinate iron nitrosyls<sup>8,9</sup> and five-coordinate cobalt nitrosyls.<sup>36</sup> An off-axis tilt of 8° in oxyCoMb has been deduced from EPR measurements,<sup>37</sup> but possibly in a different sense than that seen here. The Co–O<sub>2</sub> bond is tilted off the normal to the porphyrin plane by 2.7°. The two Co–N<sub>p</sub> bonds in the direction of the tilt are 1.9752(20) and 1.9756(21) Å (average 1.9754(3) Å), whereas the two Co–N<sub>p</sub> bonds opposite the tilt are 1.9784(20) and 1.9814(21) Å (average = 1.9802(18) Å). The differences, while only marginally statistically significant, are strongly suggestive, given the clear evidence of the phenomenon observed in the NO complexes. It is to be recognized that the similarities of O<sub>2</sub> and NO as ligands have long been noted.<sup>38,39</sup>

The top portion of Scheme 1 pictorially summarizes the coordination group geometry of  $[\text{Co}(\text{TpivPP})(1\text{-EtIm})(\text{O}_2)]$  determined at differing conditions. The scheme also provides a comparison of the cobalt oxygen structures with that reported previously for the analogous iron derivative (determined at 297 K).<sup>40</sup> The lower portion of Scheme 1 illustrates the relative orientations of the imidazole and the bent M–O<sub>2</sub> ligand with respect to the orientation of the M–N<sub>p</sub> directions of the

porphyrin core. Bisecting oxygen orientations are found for both cobalt and iron, but significant ordering of the O<sub>2</sub> position can be observed only in the cobalt systems. It can be noted that the orientation of the axial ligands shows small systematic shifts as this cobalt system is warmed (left to right, first four panels). The favored orientation of the axial O<sub>2</sub> ligand appears to approach that of exactly bisecting the bracketing Co–N<sub>p</sub> bonds, whereas the imidazole orientation tends toward eclipsing a Co–N<sub>p</sub> bond. The orientation of the major Co–O–O plane is approximately perpendicular to the imidazole plane with dihedral angles between 71 and 80°. This favored orientation may reflect modest  $\pi$  donation from the trans imidazole. The iron system shows a similar preference for the relative orientation of the Fe–O–O plane and the imidazole plane.

The bonding between the metal and the dioxygen ligand is expected to be qualitatively similar in the iron and cobalt derivatives. With the bent, end on (Pauling model) structure, bonding involves the two  $\pi^*$  orbitals on O<sub>2</sub> with the  $d_z^2$  and one of the metal  $d_x$  orbitals. Overlap of  $d_z^2$  and one  $\pi^*$  orbital leads to the  $\sigma$  bond, and overlap of the other  $\pi^*$  orbital with a metal  $d_x$  leads to the M–O<sub>2</sub>  $\pi$  bond. The singly occupied  $d_z^2$  orbital in cobalt leads to significant charge donation to O<sub>2</sub> and the formulation of a Co(III)–(O<sub>2</sub><sup>−</sup>) superoxide species. This is clearly supported by the EPR spectra<sup>41,42</sup> that indicates that the unpaired electron resides in a  $\pi^*$  antibonding molecular orbital predominantly localized on dioxygen.<sup>43</sup> The possible formulation of the oxyiron complexes as Fe(III)–(O<sub>2</sub><sup>−</sup>) has been more contentious starting from the Pauling/Weiss debate<sup>44,45</sup> and continuing to the present time.<sup>43b,46,47</sup>

The bond between iron and oxygen is a stronger bond than that in the cobalt system (M–O<sub>2</sub> is 0.15 Å shorter in iron) and reflects a significantly stronger  $\pi$  bond in the iron systems. This is clearly shown not only by the distance but by the M–O<sub>2</sub> stretching frequencies. The Co–O stretch ( $\nu(\text{Co–O})$ ) observed in both oxyCoMb (538 cm<sup>−1</sup>) and  $[\text{Co}(\text{TpivPP})(1\text{-MeIm})(\text{O}_2)]$  (516 cm<sup>−1</sup>) can be compared to  $\nu(\text{Fe–O})$  in oxyFeMb (570 cm<sup>−1</sup>) and  $[\text{Fe}(\text{TpivPP})(1\text{-MeIm})(\text{O}_2)]$  (568 cm<sup>−1</sup>).<sup>46,48</sup> Both the lower  $\nu(\text{M–O})$  and  $\nu(\text{O–O})$ <sup>49</sup> in

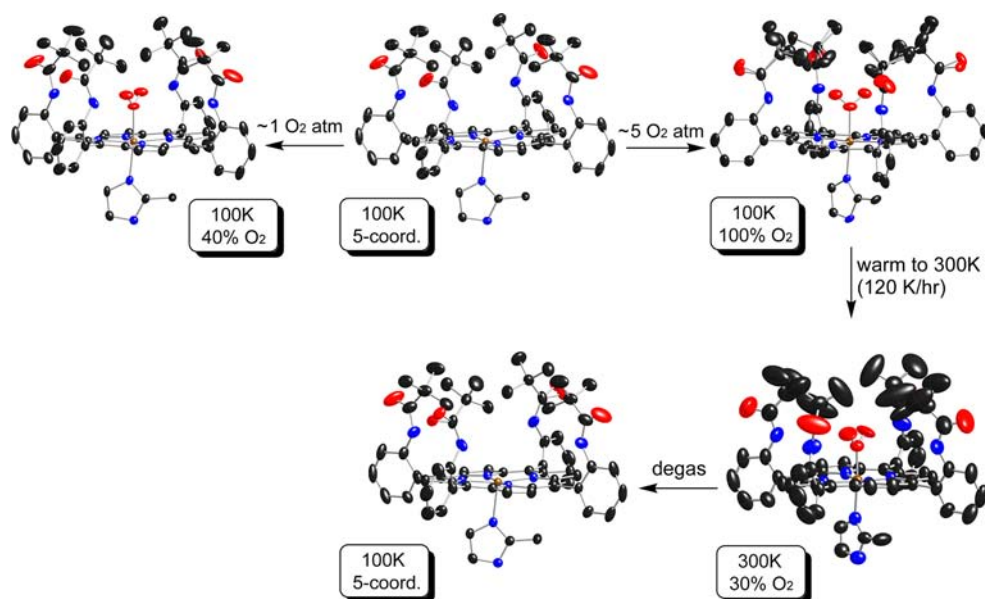


**Figure 3.** Thermal ellipsoid diagrams of  $[\text{Co}(\text{TpivPP})(2\text{-MeHIm})]$  and its oxygen adducts, showing reaction conditions and routes. The temperature and corresponding oxygen occupancy (or coordinate conditions) are given in highlighted boxes. In all species, the axial imidazole is disordered over two positions related by the required 2-fold symmetry axis, but only one orientation is shown. All thermal ellipsoids are contoured at the 50% probability level. The reaction transitions shown by arrows give the differing apparent thermal motions for the same crystalline specimen. The two diagrams for five-coordinate  $[\text{Co}(\text{TpivPP})(2\text{-MeHIm})]$  represent independent determinations of two distinct crystals. Hydrogens are omitted for clarity.

oxyCoMb and small molecule analogues compared to iron suggest that the net negative charge on the coordinated dioxygen is smaller in the iron species than in the cobalt species.<sup>50</sup> In addition, DFT calculation indicated that the interaction between the distal histidine and the oxygen ligand in oxyCoMb and oxyMb is stronger for the cobalt complex than for the iron one, consistent with larger superoxide ion character of the bound  $\text{O}_2$  in cobalt.<sup>25</sup> Thus, it can be expected that the higher negative charge on “ $\text{Co}(\text{III})\text{-O}_2^-$ ” would induce larger dipole–dipole interactions between the terminal oxygen atom and the picket amides, and result in less ligand oscillation and picket orientational disorder. This has been observed in a series of iron and cobalt oxygen basket handle derivatives where the cobalt derivatives are more sensitive to changes in the basket sizes.<sup>51</sup> It is most clearly observed in a porphyrin system where EPR showed much reduced mobility of the  $\text{Co}\text{-O}_2$  when a single amide group, similar to those in a picket fence porphyrin, was present.<sup>6a</sup> Although hydrogen bonding was suggested, the geometry is much more in line with a dipole–dipole interaction.<sup>6a</sup>

**In Situ Reversible Oxygenation Reactions of  $[\text{Co}(\text{TpivPP})(2\text{-MeHIm})]$ .** We have previously reported the synthesis and structural characterization of five-coordinate  $[\text{Co}(\text{TpivPP})(2\text{-MeHIm})]$ ,<sup>12</sup> the precursor to the six-coordinate oxygen derivative. However, the reaction of  $[\text{Co}(\text{TpivPP})(2\text{-MeHIm})]$  with  $\text{O}_2$  in benzene in the presence of a small amount of ethanol unexpectedly gave two different crystalline forms of a cobalt(III) product and not the desired dioxygen adduct. The photocatalyzed reaction leads to  $[\text{Co}(\text{TpivPP})(2\text{-MeHIm})(2\text{-MeIm}^-)]$  with the deprotonation of one imidazole providing charge balance. More surprising is the atropisomerization of the  $\alpha,\alpha,\alpha,\alpha$  isomer to yield  $[\text{Co}(\text{III})(\alpha,\alpha,\beta,\beta\text{-TpivPP})(2\text{-MeHIm})(2\text{-MeIm}^-)]$ . This change in conformation of the porphyrin allows for a hydrogen bonding chain in the axial ligands.<sup>12</sup>

Solid-state oxygenation reactions with single-crystal  $[\text{Co}(\text{TpivPP})(2\text{-MeHIm})]$  were then carried out. The reaction with ethanol-saturated  $\text{O}_2$  at 1 atm, conditions similar to the reaction conditions for the preparation of  $[\text{Fe}(\text{TpivPP})(2\text{-MeHIm})(\text{O}_2)]$ ,<sup>21</sup> gave a crystalline product, but only with a partial  $\text{O}_2$  occupancy. The structure determination suggested that the occupancy of coordinated dioxygen in the product was about 0.4. This is similar to the solid-state oxygenation of the  $\text{B}_{12}$  derivative cob(II)alamin, which was about 70% oxygenated under similar conditions.<sup>52</sup> These results are consistent with the known, lower, oxygen affinity of CoMb and the cobalt picket fence derivative compared to the iron analogues.<sup>11,53</sup> A fully occupied oxygen ligand and a satisfactory crystallographic refinement for  $[\text{Co}(\text{TpivPP})(2\text{-MeHIm})(\text{O}_2)]$  can be obtained by exposure of the crystals to 5 atm of oxygen for 5 days.

Further information on the dynamics of the system is provided by warming the crystal to 300 K under an  $\text{N}_2$  stream after the 100 K data collection. A significant amount of the dioxygen is lost as the oxygen occupancy decreases to 0.3 as the temperature increased. Large thermal motion for the pickets and the dioxygen ligand is seen for the refined crystal structure. The large apparent thermal motion of the dioxygen ligands is almost certainly hiding 4-fold disorder. The large thermal motion of picket atoms is also probably obscuring significant disorder of the pickets. The same crystal was then kept in a pure argon atmosphere with EtOH vapor preventing the loss of solvent. After several cycles of moderate pump and refill with solvent saturated argon, the crystal characterization showed that oxygen was totally removed and the five-coordinate  $[\text{Co}(\text{TpivPP})(2\text{-MeHIm})]$  precursor was recovered. The packing diagrams of Figure S13 illustrate the observations.

There are interesting differences in the pickets in these crystalline species. The five-coordinate precursor, in two independent determinations, has completely ordered pickets; this ordering is retained in the first partially oxygenated species.

Full oxygenation, however, leads to all pickets now disordered with all pickets displaying two differing orientations. When part of the  $O_2$  is lost at 300 K, the situation is ambiguous. Large thermal motion is probably hiding disordered pickets and almost certainly a 4-fold disordered dioxygen. Complete loss of the dioxygen leads to a fully ordered five-coordinate derivative. This can be clearly seen in the thermal ellipsoid plots given in Figure 3, where the reaction sequences are shown and all thermal ellipsoids are scaled to the 50% probability level. Additional thermal ellipsoid plots are given in Figures S14–S21.

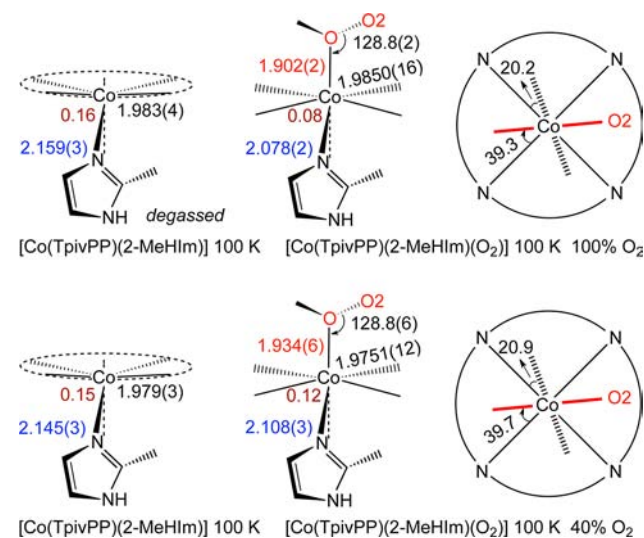
**Structure of [Co(TpivPP)(2-MeHIm)] and Its Oxygen Adducts.** A summary of structural results for [Co(TpivPP)(2-MeHIm)] and its oxygen adducts under various conditions is given in Table 3 (part B). All of these species are low spin  $S = 1/2$ . The first entry in part B gives the structural parameters for the five-coordinate complex before any oxygenation reaction. The next to final entry gives the structural parameters for a second five-coordinate crystalline sample after it had been oxygenated and then deoxygenated. We conclude that [Co(TpivPP)(2-MeHIm)] can be oxygenated/deoxygenated without significant change in crystallinity, circumstances that are not always the case.

The structure of the five-coordinate precursor is typical of previously characterized five-coordinate imidazole-ligated cobalt porphyrinates.<sup>54–57</sup> The sterically hindered 2-methylimidazole ligand had been expected to cause a modest increase in the value of the axial bond, as had been observed and discussed<sup>55</sup> in [Co(TPP)(1,2-Me<sub>2</sub>Im)] (observed 2.216 (2) Å). However, as noted previously,<sup>12</sup> in the picket fence derivative, the axial bond length does not show such an elongation. The observed distances of 2.145(3) and 2.1593(3) Å fall in the range observed for sterically unhindered imidazoles; the out-of-plane displacement is also within the range previously seen.

The changes in structure upon oxygenation are shown in the top line of Scheme 2 and in Table 3. The out-of-plane cobalt displacement decreases but does not decrease to zero; the cobalt remains on the imidazole side of the porphyrin plane. The axial Co–N(Im) bond decreases to 2.078 Å, consistent with expectations of a Co(III)–( $O_2^-$ ) formulation, but it does not decrease to the 2.02–2.03 Å value seen in the 1-EtIm derivatives (Table 3, part A). The values of the Co–O and other  $O_2$  parameters are seen to be very similar to those observed for the 1-EtIm derivative and, as discussed previously, other oxycobalt complexes as well. The limiting structures of the 1-EtIm and 2-MeHIm complexes both show one Co– $O_2$  orientation which is aligned nearly perpendicular to the imidazole plane. The differences in structure between [Co(TpivPP)(2-MeHIm)] and its oxy derivative are very similar to the differences found for deoxyCoMb and its oxy form.<sup>58</sup> Both the differences in the out-of-plane displacement and the change in the axial bond distance are slightly smaller in the picket fence derivatives.

The second line of Scheme 2 gives the structural parameters for the oxygenation product when the oxygenation was carried out at 1 atm of  $O_2$  and only partial oxygenation resulted. Two significant features resulted. At this level of oxygenation, the 2-fold axis of symmetry remains and requires two positions for the terminal oxygen and two orientations of the axial 2-MeHIm ligand. Moreover, the relative orientations of the axial ligands are the same as in the fully oxygenated derivative. However, the pickets remain completely ordered. Further oxygenation does lead to disorder in all pickets. These include the pickets that are

**Scheme 2. Formal Diagrams of Structures of Five-Coordinate [Co(TpivPP)(2-MeHIm)] and Its Oxygen Adduct [Co(TpivPP)(2-MeHIm)( $O_2$ )]<sup>a</sup>**



<sup>a</sup>The left two columns of the scheme are edge-on view of the porphyrin plane and ligands with the key parameters (distances in Å, angle in degrees) of O–O–M, M–O,  $\Delta_{24}$ , M–N<sub>prox</sub> and M–N<sub>ax</sub>. The right column of the scheme are top view of the porphyrin plane showing the projections of dioxygen (red line) and imidazole plane (dashed line) and their angles between the closest M–N<sub>p</sub> vectors.

directly pointing to the terminal oxygen atom as well as the pair of pickets that are orthogonal to the Co– $O_2$  plane. See Figures S14–S17 for detailed views. This clearly suggests that the influence of the oxygen ligand on the pickets is, at least in part, nondirectional. The interaction must be dipole–dipole in character, as the distances to the picket amides are beyond that expected for hydrogen bonding. The  $O \cdots N$  distances are in the range 4.0–4.1 Å, and the  $O \cdots H(N)$  distances are in the range  $> \sim 3.2$  Å. Calculations by Rovira and Parrinello<sup>22</sup> have indicated that the pickets provide substantial energetic stabilization for the binding of  $O_2$ . However, the energetics of the varying Co–O–O orientations and the picket orientations must be very similar.

Scheme 2 also illustrates the probable effect on the experimentally derived structural parameters when the crystalline sample is a mixture of the six-coordinate species and the five-coordinate precursor. The apparent metal ion displacement is between the two limiting values, and the apparent values of *both* axial bond distances are longer than the true values. The effects are substantial, and the observations for the cobalt system can be expected to be the general result.

**Comparison of R- and T-State Oxy Models.** The movement of iron toward the porphyrin plane upon oxygenation, along with the motion of proximal histidine, has been cited as the driving force in the mechanism of cooperative oxygen binding in the human hemoglobin.<sup>59,60</sup> The movements of iron and the proximal histidine lead to changes in the protein quaternary structure of hemoglobin that lead to the cooperativity of oxygen binding. Cooperativity is retained, but diminished, in human hemoglobin when the iron is replaced with cobalt; the Hill coefficient decreases from 2.8 to 2.2.<sup>61</sup> The difference is attributed to the fact that the Co out-of-plane displacement and subsequent movement upon oxygenation will be much smaller than that for iron, since cobalt does not

undergo a spin state change.<sup>62</sup> However, it is essential to note that the binding of dioxygen does lead to significant difference changes in model R- and T-state cobalt systems on the change from a five-coordinate to a six-coordinate species. In both [Co(TpivPP)(1-EtIm)(O<sub>2</sub>)] and [Co(TpivPP)(2-MeHIm)(O<sub>2</sub>)] the change in the out-of-plane displacement of cobalt is about 0.08 Å, with the cobalt remaining further out-of-plane in the 2-MeHIm system. But, the change in the axial Co–N(Im) bond distance is almost twice as large in that in [Co(TpivPP)(1-EtIm)(O<sub>2</sub>)]. The total change leads to half again as much motion of the axial imidazole relative to the porphyrin plane in this R-state model (0.23 Å change in the R-state system vs 0.16 Å in the T-state system).

## SUMMARY

Two different O<sub>2</sub> complexes of picket fence cobalt porphyrin, [Co(TpivPP)(R-Im)(O<sub>2</sub>)], where R-Im is either 1-ethylimidazole or the sterically hindered 2-methylimidazole, have been synthesized. The solid-state structures of the two species have been determined at a number of temperatures. Under most conditions, both axial ligands and the pickets of the porphyrin are disordered. However, crystal annealing leads to an unusual reversible phase change for [Co(TpivPP)(1-EtIm)(O<sub>2</sub>)] that provides an ordered structure and excellent structural parameters. The studies have provided distinct information on the interactions between the coordinated O<sub>2</sub> and pickets that lead to apparent mutual disorder in the solid state. The disordered pickets apparently result from the movement required to allow rotation of the O<sub>2</sub> ligand about the Co–O bond. The results also reveal the subtle effects on structural parameters from an incomplete oxygenation reaction in the single crystal.

## ASSOCIATED CONTENT

### Supporting Information

Line drawing of [Co(TpivPP)(1-EtIm)(O<sub>2</sub>)], thermal ellipsoid plots and mean plane diagrams for all structures, brief description of synthesis of PF porphyrin, complete structural details for [Co(TpivPP)(1-EtIm)(O<sub>2</sub>)], complete structural details for [Co(TpivPP)(2-MeHIm)(O<sub>2</sub>)], complete structural details for [Co(TpivPP)(2-MeHIm)], and crystallographic information files (CIF). This material is available free of charge via the Internet at <http://pubs.acs.org>.

## AUTHOR INFORMATION

### Corresponding Author

Scheidt.1@nd.edu

### Notes

The authors declare no competing financial interest.

## ACKNOWLEDGMENTS

We thank the National Institutes of Health for support of this research under Grant GM-38401 to W.R.S.

## REFERENCES

- (1) *The Smallest Biomolecules: Diatomics and Their Interactions with Heme Proteins*; Ghosh, A., Ed.; Elsevier: Amsterdam, 2008.
- (2) (a) Debrunner, P. G. In *Iron Porphyrins, Part 3*; Lever, A. B. P., Gray, H. B., Eds.; VCH Publishers: New York, 1989; pp 177–181. (b) Boso, B.; Debrunner, P. G.; Wagner, G. C.; Inubushi, T. *Biochim. Biophys. Acta* **1984**, *791*, 244. (c) Winkler, H. *Hyperfine Interact.* **2002**, *199/200*, 199.

(3) Abbreviations: N<sub>p</sub>, porphyrinato nitrogen; N<sub>ax</sub>, nitrogen of axial ligands; M, center metal atom; N<sub>im</sub>, nitrogen of imidazole ligands; Δ<sub>24</sub>, displacement of metal atom from the 24-atom mean plane; EPR, electron paramagnetic resonance; Mb, myoglobin; TpivPP, dianion of α,α,α,α-tetrakis(*o*-pivalamidophenyl)porphyrin; 1-MeIm, 1-methylimidazole; 1-EtIm, 1-ethylimidazole; 2-MeHIm, 2-methylimidazole; R-Im, generalized imidazole; Py, pyridine; Mb, myoglobin; Hb, hemoglobin; CoMb, cobalt substituted myoglobin; CoHb, cobalt substituted hemoglobin.

(4) Spartalian, K.; Lang, G.; Collman, J. P.; Gagne, R. R.; Reed, C. A. *J. Chem. Phys.* **1975**, *63*, 5375.

(5) Godbout, N.; Sanders, L. K.; Salzmann, R.; Havlin, R. H.; Wojdelski, M.; Oldfield, E. *J. Am. Chem. Soc.* **1999**, *121*, 3829.

(6) (a) Walker, F. A.; Bowen, J. *J. Am. Chem. Soc.* **1985**, *107*, 7632. (b) Odo, J.; Imai, H.; Kyuno, E.; Nakamoto, K. *J. Am. Chem. Soc.* **1988**, *110*, 742. (c) Dube, H.; Kasumaj, B.; Calle, C.; Saito, M.; Jeschke, G.; Diederich, F. *Angew. Chem., Int. Ed.* **2008**, *47*, 2600.

(7) Bowen, J. H.; Shokhirev, N. V.; Raitsimring, A. M.; Buttlare, D. H.; Walker, F. A. *J. Chem. Phys. B* **1997**, *101*, 8683.

(8) Silvernail, N. J.; Pavlik, J. W.; Noll, B. C.; Schulz, C. E.; Scheidt, W. R. *Inorg. Chem.* **2008**, *47*, 912–920.

(9) Silvernail, N. J.; Barabanshikov, A.; Sage, J. T.; Noll, B. C.; Scheidt, W. R. *J. Am. Chem. Soc.* **2009**, *131*, 2131–2140.

(10) Li, J.; Noll, B. C.; Oliver, A. G.; Schulz, C. E.; Scheidt, W. R. Manuscripts in preparation. Structural data for three [Fe(TpivPP)(R-Im)(O<sub>2</sub>)] derivatives (R-Im = 1-MeIm, 1-EtIm, and 2-MeHIm) at temperatures between 100 and 300 K have been obtained. At 100 K, all structures are in C2/c and show four-fold positional disorder at the terminal oxygen (O<sub>2</sub>). Systematically temperature-dependent Mössbauer spectroscopy has been conducted on [Fe(TpivPP)(R-Im)(O<sub>2</sub>)] (R-Im = 1-MeIm, 1-EtIm, and 2-MeHIm).

(11) Collman, J. P.; Brauman, J. I.; Doxsee, K. M.; Halbert, T. R.; Hayes, S. E.; Suslick, K. S. *J. Am. Chem. Soc.* **1978**, *100*, 2761.

(12) Li, J.; Noll, B. C.; Oliver, A. G.; Ferraudi, G.; Lappin, A. G.; Scheidt, W. R. *Inorg. Chem.* **2010**, *49*, 2398.

(13) Sheldrick, G. M. *Acta Crystallogr.* **2008**, *A64*, 112.

(14)  $R_1 = \sum ||F_o| - |F_c|| / \sum |F_o|$  and  $wR_2 = \{ \sum [w(F_o^2 - F_c^2)^2] / \sum [wF_o^4] \}^{1/2}$ . The conventional R-factors R<sub>1</sub> are based on F, with F set to zero for negative F<sup>2</sup>. The criterion of F<sup>2</sup> > 2σ(F<sup>2</sup>) was used only for calculating R<sub>1</sub>. R-factors based on F<sup>2</sup> (wR<sub>2</sub>) are statistically about twice as large as those based on F, and R-factors based on ALL data will be even larger.

(15) Sheldrick, G. M. *Program for Empirical Absorption Correction of Area Detector Data*; Universität Göttingen: Germany, 1996.

(16) Sheldrick, G. M. *twinabs*; Universität Göttingen: Germany, 2005.

(17) (a) Macrae, C. F.; Edgington, P. R.; McCabe, P.; Pidcock, E.; Shields, G. P.; Taylor, R.; Towler, M.; van de Streek, J. *J. Appl. Crystallogr.* **2006**, *39*, 453. (b) Bruno, I. J.; Cole, J. C.; Edgington, P. R.; Kessler, M. K.; Macrae, C. F.; McCabe, P.; Pearson, J.; Taylor, R. *Acta Crystallogr.* **2002**, *B58*, 389. (c) Taylor, R.; Macrae, C. F. *Acta Crystallogr.* **2001**, *B57*, 815.

(18) Hu, C.; Roth, A.; Ellison, M. K.; An, J.; Ellis, C. M.; Schulz, C. E.; Scheidt, W. R. *J. Am. Chem. Soc.* **2005**, *127*, 5675.

(19) Kitazawa, T.; Nishikiori, S.-I.; Kuroda, R.; Iwamoto, T. *J. Chem. Soc., Dalton Trans.* **1994**, 1029.

(20) Jameson, G. B.; Rodley, G. A.; Robinson, W. T.; Gagne, R. R.; Reed, C. A.; Collman, J. P. *Inorg. Chem.* **1978**, *17*, 850.

(21) Jameson, G. B.; Molinaro, F. S.; Ibers, J. A.; Collman, J. P.; Brauman, J. I.; Rose, E.; Suslick, K. S. *J. Am. Chem. Soc.* **1980**, *102*, 3224.

(22) Rovira, C.; Parrinello, M. *Chem.—Eur. J.* **1999**, *5*, 250.

(23) Bondi, A. *J. Phys. Chem.* **1964**, *68*, 441.

(24) (a) Nasri, H.; Goodwin, J. A.; Scheidt, W. R. *Inorg. Chem.* **1990**, *29*, 185. (b) Nasri, H.; Wang, Y.; Huynh, B. H.; Scheidt, W. R. *J. Am. Chem. Soc.* **1991**, *113*, 717. (c) Nasri, H.; Wang, Y.; Huynh, B. H.; Walker, F. A.; Scheidt, W. R. *Inorg. Chem.* **1991**, *30*, 1483. (d) Nasri, H.; Haller, K. J.; Wang, Y.; Huynh, B. H.; Scheidt, W. R. *Inorg. Chem.* **1992**, *31*, 3459. (e) Nasri, H.; Ellison, M. K.; Chen, S.; Huynh, B. H.;

- Scheidt, W. R. *J. Am. Chem. Soc.* **1997**, *119*, 6274. (f) Nasri, H.; Ellison, M. K.; Krebs, C.; Huynh, B. H.; Scheidt, W. R. *J. Am. Chem. Soc.* **2000**, *122*, 10795. (g) Nasri, H.; Ellison, M. K.; Shang, M.; Schulz, C. E.; Scheidt, W. R. *Inorg. Chem.* **2004**, *43*, 2932.
- (25) Degtyarenko, I.; Nieminen, R. M.; Rovira, C. *Biophys. J.* **2006**, *91*, 2024.
- (26) Rodley, G. A.; Robinson, W. T. *Nature* **1972**, 235, 438.
- (27) Calligaris, M.; Nardin, G.; Randaccio, L. *J. Chem. Soc., Dalton Trans.* **1973**, 419.
- (28) Jameson, G. B.; Robinson, W. T.; Rodley, G. A. *J. Chem. Soc., Dalton Trans.* **1978**, 191.
- (29) Gall, R. S.; Rogers, J. F.; Schaefer, W. P.; Christoph, G. G. *J. Am. Chem. Soc.* **1976**, *98*, 5135.
- (30) Gall, R. S.; Rogers, J. F.; Schaefer, W. P.; Christoph, G. G. *Inorg. Chem.* **1980**, *19*, 340.
- (31) Avdeef, A.; Schaefer, W. P. *J. Am. Chem. Soc.* **1976**, *98*, 5153.
- (32) Gall, R. S.; Schaefer, W. P. *Inorg. Chem.* **1976**, *15*, 2758.
- (33) Doppelt, P.; Fischer, J.; Richard, L.; Weiss, R. *Nouv. J. Chim.* **1987**, *11*, 357.
- (34) Ellison, M. K.; Scheidt, W. R. *J. Am. Chem. Soc.* **1997**, *119*, 7404.
- (35) Scheidt, W. R.; Duval, H. F.; Neal, T. J.; Ellison, M. K. *J. Am. Chem. Soc.* **2000**, *122*, 4651.
- (36) Ellison, M. K.; Scheidt, W. R. *Inorg. Chem.* **1998**, *37*, 382.
- (37) Hori, H.; Ikeda-Saito, M.; Yonetani, T. *Nature* **1980**, 288, 501.
- (38) Scheidt, W. R.; Hoard, J. L. *J. Am. Chem. Soc.* **1973**, *95*, 8281.
- (39) Schenk, G.; Pau, M. Y. M.; Solomon, E. I. *J. Am. Chem. Soc.* **2004**, *126*, 505.
- (40) We have carried out a number of multiple-temperature structure determinations for [Fe(TpivPP)(R-Im)(O<sub>2</sub>)] derivatives.<sup>10</sup> In most cases, the O<sub>2</sub> ligand is disordered over four positions.
- (41) Walker, F. A. *J. Am. Chem. Soc.* **1970**, *92*, 4235.
- (42) (a) Hoffman, B. M.; Diemente, D. L.; Basolo, F. *J. Am. Chem. Soc.* **1970**, *92*, 61. (b) Getz, D.; Melemud, E.; Silver, B. C.; Dori, Z. *J. Am. Chem. Soc.* **1975**, *97*, 3846.
- (43) (a) Wayland, B. B.; Minkiewix, J. V.; Abd-Elmageed, M. E. *J. Am. Chem. Soc.* **1974**, *96*, 2795. (b) Dedieu, A.; Rohmer, M.-M.; Veillard, A. *J. Am. Chem. Soc.* **1976**, *98*, 5789. (c) Reed, C. A.; Cheung, S. K. *Proc. Natl. Acad. Sci. U.S.A.* **1977**, *74*, 1780.
- (44) Pauling, L. *Nature* **1964**, *203*, 182.
- (45) Weiss, J. J. *Nature* **1964**, *202*, 84; **1964**, *203*, 183.
- (46) Burke, J. M.; Kincaid, J. R.; Peters, S.; Gagne, R. R.; Collman, J. P.; Spiro, T. G. *J. Am. Chem. Soc.* **1978**, *100*, 6083.
- (47) Chen, H.; Ikeda-Saito, M.; Shaik, S. *J. Am. Chem. Soc.* **2008**, *130*, 14778. This reference details additional information on the debate.
- (48) (a) Tsubaki, M.; Yu, N.-T. *Proc. Natl. Acad. Sci. U.S.A.* **1981**, *78*, 3581. (b) Mackin, H. C.; Tsubaki, M.; Yu, N.-T. *Biophys. J.* **1983**, *41*, 349.
- (49) Collman, J. P.; Brauman, J. I.; Halbert, T. R.; Suslick, K. S. *Proc. Natl. Acad. Sci. U.S.A.* **1976**, *73*, 3333.
- (50) Nakamoto, K.; Paeng, I. R.; Kuroi, T.; Isobe, T.; Oshio, H. *J. Mol. Struct.* **1988**, *189*, 293.
- (51) Collman, J. P.; Zhang, X.; Wong, K.; Braumkna, J. L. *J. Am. Chem. Soc.* **1994**, *116*, 6245.
- (52) Hohenester, E.; Kratky, C.; Krautler, B. *J. Am. Chem. Soc.* **1991**, *113*, 4523.
- (53) (a) Hoffman, B. M.; Petering, D. H. *Proc. Natl. Acad. Sci. U.S.A.* **1970**, *67*, 637. (b) Chien, J. C. W.; Dickinson, L. C. *Proc. Natl. Acad. Sci. U.S.A.* **1972**, *69*, 2783.
- (54) Scheidt, W. R. *J. Am. Chem. Soc.* **1974**, *96*, 90–94.
- (55) Dwyer, P. N.; Madura, P.; Scheidt, W. R. *J. Am. Chem. Soc.* **1974**, *96*, 4815.
- (56) Little, R. G.; Ibers, J. A. *J. Am. Chem. Soc.* **1974**, *96*, 4452.
- (57) Jene, P. G.; Ibers, J. A. *Inorg. Chem.* **2000**, *39*, 5796.
- (58) Brucker, E. A.; Olson, J. S.; Phillips, G. N., Jr.; Dou, Y.; Ikeda-Saito, M. *J. Biol. Chem.* **1996**, *271*, 25419.
- (59) (a) Perutz, M. F. *Nature* **1970**, *228*, 726. (b) Perutz, M. F. *Br. Med. Bull.* **1976**, *32*, 195. (c) Perutz, M. F.; Wilkinson, A. J.; Paoli, M.; Dodson, G. G. *Annu. Rev. Biophys. Biomol. Struct.* **1998**, *27*, 1.
- (60) The R- and T-states of hemoglobin in both the five- and six-coordinate forms have been modeled by changing the axial imidazole from an unhindered to a hindered imidazole.
- (61) Yonetani, T.; Yamamoto, H.; Woodrow, G. V., III. *J. Biol. Chem.* **1974**, *249*, 682.
- (62) Hoard, J. L.; Scheidt, W. R. *Proc. Natl. Acad. Sci. U.S.A.* **1973**, *70*, 3919.